Physics Letters B 843 (2023) 138007

Contents lists available at ScienceDirect

Physics Letters B

journal homepage: www.elsevier.com/locate/physletb

Suppression of Coulomb-nuclear interference in the near-barrier elastic scattering of ^{17}Ne from ^{208}Pb

J.D. Ovejas [a], I. Martel [b,*], D. Dell'Aquila [c,q], L. Acosta [e], J.L. Aguado [b], G. de Angelis [f], M.J.G. Borge [a], J.A. Briz [a], A. Chbihi [g], G. Colucci [h], C. Díaz-Martín [b], P. Figuera [d], D. Galaviz [i], C. García-Ramos [b], J.A. Gómez-Galán [b], C.A. Gonzales [b], N. Goyal [g], N. Keeley [j], K.W. Kemper [k], T. Kurtukian Nieto [l], D.J. Malenica [m], M. Mazzocco [n,o], D. Nurkić [p], A.K. Orduz [g], A. Ortiz [g], L. Palada [m], C. Parascandolo [q], A. Di Pietro [d], A.M. Rodriguez [b], K. Rusek [h], F. Salguero [b], A.M. Sánchez-Benítez [r], M. Sánchez-Raya [b], J. Sánchez-Segovia [b], N. Soić [m], F. Soramel [n,o], M. Stanoiu [s], O. Tengblad [a], N. Vukman [m], M. Xarepe [i]

[a] *Instituto de Estructura de la Materia, CSIC, 28006 Madrid, Spain*
[b] *Science and Technology Research Centre, University of Huelva, 21071 Huelva, Spain*
[c] *Dipartimento di Fisica Ettore Pancini, University of Naples Federico II, Naples, Italy*
[d] *INFN-Laboratori Nazionali del Sud, 95123 Catania, Italy*
[e] *Instituto de Física, UNAM, Mexico*
[f] *INFN-National Laboratories of Legnaro, 35020 Legnaro (PD), Italy*
[g] *Grand Accélérateur National d'Ions Lourds, BP 55027 - 14076 Caen, Cedex 05, France*
[h] *Heavy Ion Laboratory, University of Warsaw, ul. Pasteura 5a, 02-093 Warsaw, Poland*
[i] *LIP, Lisboa, Portugal*
[j] *National Centre for Nuclear Research, ul. Andrzeja Sołtana 7, 05-400 Otwock, Poland*
[k] *Department of Physics, The Florida State University, Tallahassee, FL 32306, USA*
[l] *Centre d'Etudes Nucléaires de Bordeaux Gradignan, Chemin du Solarium, Gradignan F-33175, France*
[m] *Rudjer Bošković Institute, Bijenička cesta 54, HR-10000 Zagreb, Croatia*
[n] *Dipartimento di Fisica e Astronomia, Università di Padova, via F. Marzolo 8, I-35131 Padova, Italy*
[o] *INFN-Sezione di Padova, via F. Marzolo 8, I-35131 Padova, Italy*
[p] *Department of Physics, Faculty of Science, University of Zagreb, Zagreb, Croatia*
[q] *INFN-Naples, Italy*
[r] *Centro de Estudios Avanzados en Física, Matemáticas y Computación, University of Huelva, 21071 Huelva, Spain*
[s] *IFIN-HH PO-BOX MG-6, 76900 Bucharest Magurele, Romania*

ARTICLE INFO

Article history:
Received 5 February 2023
Received in revised form 27 April 2023
Accepted 6 June 2023
Available online 9 June 2023
Editor: B. Blank

Keywords:
Direct nuclear reactions
Radioactive beams
Optical model
Elastic scattering

ABSTRACT

The proton drip-line nucleus ^{17}Ne is considered a good candidate for a Borromean two-proton halo with a ^{15}O + p + p structure. Angular distributions of the elastic scattering and inclusive ^{15}O production for a 136 MeV ^{17}Ne beam incident on a ^{208}Pb target were measured for the first time at the SPIRAL1 facility, GANIL. Use of the GLORIA detector array allowed high-resolution data over a wide angular range from 20° up to 95° in the laboratory frame to be obtained. The elastic scattering angular distribution shows similarities with those for both ^{6}He and ^{20}Ne at equivalent collision energies with respect to the corresponding Coulomb barriers, exhibiting the suppression of the Coulomb rainbow peak characteristic of strong coupling. Optical model and coupled channel fits suggest that this is due to a combination of coupling to low-lying quadrupole resonances and Coulomb dipole coupling to the low-lying continuum, although their relative importance depends on the relevant $B(E2)$ values which remain to be firmly determined.

© 2023 The Authors. Published by Elsevier B.V. This is an open access article under the CC BY license (http://creativecommons.org/licenses/by/4.0/). Funded by SCOAP[3].

1. Introduction

Halo nuclei are exotic states of nuclear matter consisting of one or more weakly-bound valence nucleons spatially decoupled

* Corresponding author.
E-mail address: imartel@uhu.es (I. Martel).

https://doi.org/10.1016/j.physletb.2023.138007
0370-2693/© 2023 The Authors. Published by Elsevier B.V. This is an open access article under the CC BY license (http://creativecommons.org/licenses/by/4.0/). Funded by SCOAP[3].

from a tightly bound core [1]. The reduced binding energy favours tunnelling through the potential binding the valence nucleon(s) to the core, producing an extended density distribution, the so-called "nuclear halo", surrounding the core. Known halo systems have a large rms matter radius and a significant fraction of the Coulomb dipole strength $B(E1)$ is found close to the breakup threshold. Several neutron halo systems have been identified during the last few decades, and typical examples are: ^{6}He (2n) [1,2], ^{11}Li (2n) [1,2], and ^{11}Be (1n) [3,4]. Proton halo candidates are less common; based on experimental evidence proton halo formation has been proposed only for ^{8}B (1p) [5–8] and ^{17}Ne (2p) [9–11].

Reactions induced by halo nuclei exhibit special features due to the rôle played by the low binding energy and the coupling to the continuum [12,13]. At Coulomb barrier energies the dynamics of halo nuclei are dominated by couplings between the elastic channel and inelastic scattering, nucleon transfer and breakup. The near-barrier elastic scattering of ^{6,8}He, ^{11}Li and ^{11}Be has been extensively studied [14–26]. A common feature is that the measured angular distributions for elastic scattering from heavy targets exhibit a long-range absorption pattern which reduces the yield from relatively forward angles, and the usual Coulomb rainbow peak is either completely absent or heavily suppressed.

Experimental information on proton halo scattering at low energies is relatively sparse, and only ^{8}B has been studied so far, with data sets for ^{12}C [27], ^{27}Al [28], ^{58}Ni [29], ^{64}Zn [30], ^{120}Sn [31] and ^{208}Pb [32,33,35,36] targets. Breakup coupling effects on the elastic scattering appear modest, the data for higher incident energies and/or lighter targets [27,28,30] exhibiting standard Fresnel-type angular distributions. While the Coulomb rainbow peak does seem to be suppressed for the other cases [29,31,33], this remains to be confirmed experimentally for the ^{58}Ni and ^{208}Pb targets due to the relatively poor statistics obtained, while the coupling effect for the ^{120}Sn target is somewhat smaller than for the neutron halo nucleus ^{6}He scattered from the same target [34]. Taken as a whole the available data suggest that heavy targets and/or incident energies within a few MeV of the Coulomb barrier are required for a significant coupling effect, in agreement with continuum discretised coupled channels (CDCC) predictions [37].

The ^{17}Ne nucleus is the most neutron-deficient of the neon isotope chain, lying at the proton drip-line. Its two-proton separation energy ($S_{2p} = 933.1 \pm 0.6$ keV [38]) is much smaller than the single-proton separation energy ($S_p = 1464 \pm 5$ keV [38]), and the ^{16}F subsystem is unbound by 535 keV with respect to proton emission. With a first excited state at an energy of 5.18 MeV ^{15}O makes a reasonable core, and in this picture the two valence protons are in an admixture of $(2s_{1/2})^2$ and $(1d_{5/2})^2$ configurations. Thus ^{17}Ne is expected to exhibit a Borromean two-proton halo [9,10] with a ^{15}O + p + p structure, analogous to the well known two-neutron halo nuclei in ^{6}He and ^{11}Li. The presence of a halo is also inferred from the interaction cross sections [39,40], the transverse-momentum distributions for two-proton removal [41], and the beta decay [42].

However, the existence of a two-proton halo in ^{17}Ne has been the subject of debate from both theoretical and experimental points of view (see, e.g., [43] for a discussion using a three-body model). A recent study [11] using quasi-free knockout reactions found the $(1s_{1/2})^2$ contribution to the ground state accounting for only 35±3%, from which only a modest halo effect was inferred. It is therefore important to establish the strength of the breakup coupling influence on the elastic scattering of ^{17}Ne: Does it compare to that seen for neutron halo nuclei or is it more modest, as appears to be the case for ^{8}B? Studies with both ^{8}B and ^{6}He projectiles [37,44] have emphasised the importance of an incident energy close to the Coulomb barrier together with a heavy target to provide a large Coulomb field if coupling effects are to be maximised. The Coulomb barrier scattering of ^{17}Ne has not been previously studied (see [45] for a review), and in this work we present a high-precision measurement of the elastic scattering angular distribution of ^{17}Ne from the heavy target ^{208}Pb together with the inclusive ^{15}O production cross section, covering the angular range $\theta_{\rm lab} = 20^\circ$ to 95°.

2. Experiment and data analysis

The experiment was carried out at the SPIRAL1 facility of GANIL, France. A pure ^{17}Ne beam was produced by fragmentation of a ^{20}Ne driver beam on a graphite target, followed by post acceleration by the CIME cyclotron to an energy of 136 MeV and delivery to the reaction chamber with an average intensity of 1.5×10^4 pps. Scattered ^{17}Ne nuclei and other reaction fragments were registered by the GLORIA (GLObal Reaction Array) detection system [46], consisting of six charged particle telescopes, each formed of a thin (40 μm) Double-Sided-Silicon-Strip-Detector (DSSSD) followed by a thick (500 μm) silicon pad. The pad covered the entire active area of the DSSSD and was used to measure the residual energy of ions punching through the DSSSD. Two telescopes were placed in the forward hemisphere, covering angles from 15° to 62° in the laboratory frame, two in the backward hemisphere (117°-165°), one above (82°-128°) and one below (52°-97°) the horizontal plane identified by the centres of the forward and backward telescopes. Pairs of contiguous telescopes had an angular overlap of at least 10°. The target was a 1.2 mg/cm^2 thick self-supporting ^{208}Pb foil, and was rotated by about 60° with respect to the beam axis to allow the detection of particles around 90°, enabling elastically scattered ^{17}Ne nuclei to be measured without gaps over a laboratory angle range from 15° to 165° with a resolution of about 3°.

The silicon pads were energy calibrated using a standard triple alpha source containing a mixture of ^{239}Pu, ^{241}Am, and ^{244}Cm. Elastically scattered ^{17}Ne nuclei punching through the first detection stage were subsequently used individually to perform the energy calibration for each vertical and horizontal strip in the array. In the calculation of the elastic scattering energy, losses due to the detector dead layers and interaction with the target material before and after the scattering were carefully accounted for. This calculation was repeated for each pixel in a strip to account for the different effective target thicknesses traversed by the elastically scattered ^{17}Ne nuclei before detection. The energy deposited in the strip was finally calculated by relying on the calibration of the corresponding silicon pad. An energy calibration unaffected by the non-uniform thickness of the DSSSD was thus obtained. The average energy resolution achieved was around 200 keV. Throughout the experiment a test signal of calibrated amplitude and fixed frequency (≈ 2 Hz) was sent to all preamplifiers to monitor the stability of the electronics and its efficiency and the dead time, which was found to be negligible due to the low intensity of the radioactive beam.

Elastically scattered ^{17}Ne nuclei were identified using the $E_{\rm DSSSD}$ versus $E_{\rm DSSSD} + E_{\rm pad}$ distributions. $E_{\rm DSSSD}$ denotes the energy deposited by the ion in a given vertical and horizontal strip of the first detection layer and $E_{\rm pad}$ its residual energy, deposited in the corresponding silicon pad where the ion stopped. The collected statistics enabled the identification to be performed pixel-by-pixel, minimising the loss of resolution due to any non-uniformity in the thickness of the DSSSDs. Fig. 1 shows a typical calibrated $E_{\rm DSSSD}$ vs. $E_{\rm DSSSD} + E_{\rm pad}$ distribution for a pixel in one of the forward telescopes at $\theta_{\rm lab} \approx 60^\circ$. The locus of elastically scattered ^{17}Ne ions, indicated by the red line, is identified with excellent separation from the neighbouring loci for fluorine and oxygen isotopes. The corresponding kinematic curve of the elastic events is shown in Fig. 2.

The analysis was restricted to events detected in time coincidence with the beam radio-frequency. In this way, spurious events

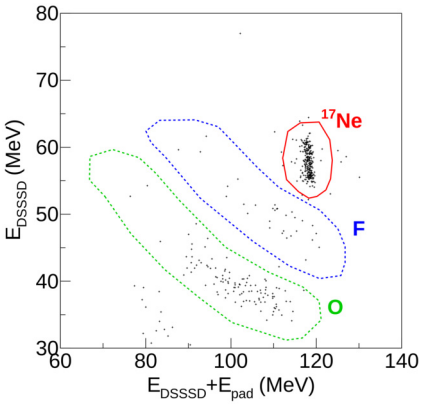

Fig. 1. Energy-loss (E_{DSSSD}) vs. total energy ($E_{\mathrm{DSSSD}} + E_{\mathrm{pad}}$) distribution of outgoing fragments for a pixel in the forward hemisphere of the GLORIA array ($\theta_{\mathrm{lab}} = 60°$). The locus of elastically scattered ^{17}Ne nuclei is identified by the red line. Dashed blue and green lines denote the loci of fluorine and oxygen ions respectively.

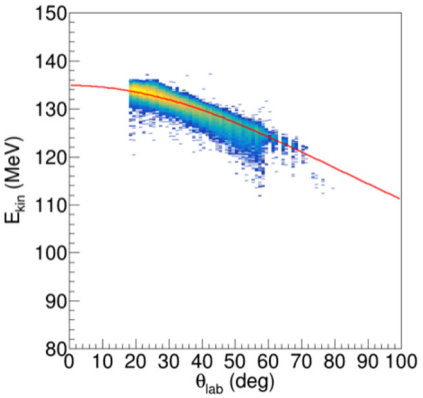

Fig. 2. Kinematics plot (Energy vs. scattering angle) of elastic events corrected for energy losses in the target and detector dead layers. The red line denotes a calculation of the kinematics. Energy resolution is about 120 keV at the most forward angles.

were removed. The ^{17}Ne + ^{208}Pb elastic scattering yield was obtained pixel-by-pixel using suitable identification cuts, as shown in Fig. 1. Considerable care was devoted to correcting the positioning of the detection array for possible small beam misalignment at the target position. This is a crucial step, since the elastic scattering cross section varies rapidly with scattering angle, particularly at forward angles. The position of the beam on the target, and therefore the detection angle for each pixel in the array, was determined by minimising the difference between the differential elastic scattering angular distribution measured by the two telescopes positioned in the forward hemisphere. The error function in the beam position parameter space led to a unique absolute minimum. After determining the beam position on target, a detailed simulation of the GLORIA array was carried out to estimate angle and solid angle for each pixel. The elastic scattering angular distribution was then obtained as follows:

$$\frac{\sigma_{\mathrm{el}}(\theta_{\mathrm{cm},i})}{\sigma_{\mathrm{Ruth}}(\theta_{\mathrm{cm},i})} = k\frac{N_{\mathrm{el},i}}{\Delta\Omega_i \sin^4\left(\frac{\theta_{\mathrm{cm},i}}{2}\right)} \quad (1)$$

where $N_{\mathrm{el},i}$ is the yield of elastically scattered ^{17}Ne measured by the i-th pixel, $\theta_{\mathrm{cm},i}$ and $\Delta\Omega_i$ are respectively its angle and solid angle in the centre-of-mass reference frame, and k is a constant determined assuming that at small scattering angles ($\theta_{\mathrm{c.m}} = 20°–30°$) the elastic scattering cross section has the Rutherford value.

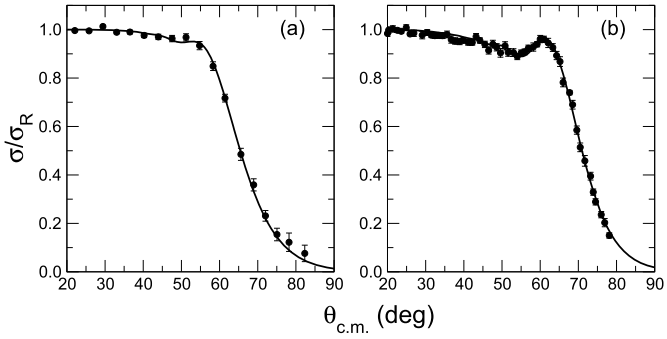

Fig. 3. (a) 136 MeV ^{17}Ne + ^{208}Pb elastic scattering angular distribution. (b) 131 MeV ^{20}Ne + ^{208}Pb [49] elastic scattering angular distribution. The solid curves denote the optical model fits described in the text.

Finally, since the elastic scattering cross section using non-polarised beams is azimuthally symmetric, measured ^{17}Ne yields and solid angles were summed over pixels at similar polar angles ($\pm 1.5°$) differing only in azimuthal angle. The statistics were thus maximised and the uncertainties of each data point reduced. The resulting elastic scattering angular distribution is plotted on Fig. 3 (a) as the filled circles.

The inclusive oxygen production cross section was obtained in a similar manner, selecting events contained within the oxygen locus (dashed green line on Fig. 1). Unfortunately, due to the low statistics and the energy spread of the ΔE detector it was not possible to obtain a clean isotopic identification. Nonetheless, due to the Borromean structure of ^{17}Ne one would expect the production of oxygen to be dominated by ^{15}O core fragments; for example, the Q value for the ^{208}Pb(^{17}Ne,^{14}O)^{211}Po stripping is -0.823 MeV whereas the optimum Q value for this reaction is approximately -20 MeV. The resulting angular distribution is plotted on Fig. 6 as the filled circles.

3. Comparison with other systems

The most conspicuous aspect of the ^{17}Ne + ^{208}Pb elastic scattering angular distribution plotted in Fig. 3 (a) is the suppression of the usual Coulomb rainbow peak, an unmistakable sign of strong coupling [47]. In this respect it bears a striking similarity to the near-barrier ^{6}He + ^{208}Pb elastic scattering, see, e.g., the 27 MeV ^{6}He + ^{208}Pb data of Kakuee et al. [14]. For ^{6}He this suppression of the Coulomb rainbow peak is largely due to strong $E1$ coupling to the low-lying continuum. It is thus tempting to ascribe the observed behaviour of the ^{17}Ne elastic scattering to a similar cause, particularly when it is recalled that the $1n$ and $2n$ thresholds of ^{6}He, 1710 keV and 975 keV respectively, are similar to the $1p$ and $2p$ thresholds of ^{17}Ne. However, while this is an appealing hypothesis, it is too simplistic since, for example, it has been shown [48] that for proton halo nuclei the charge on the valence particle(s) leads to a significantly larger "effective" binding energy compared to the equivalent neutron halo when considering the breakup cross section.

The ^{17}Ne + ^{208}Pb elastic scattering also closely resembles the ^{20}Ne and ^{22}Ne + ^{208}Pb elastic scattering at 131 and 132 MeV respectively [49,50], the former particularly so, see Fig. 3 (b). In these systems the strong $E2$ coupling to the collective 2_1^+ levels leads to the suppression of the Coulomb rainbow peak. The ^{20}Ne 2_1^+ level is at an excitation energy of 1634 keV and has a $B(E2) = 340$ e^{2}fm^4, the corresponding values for ^{22}Ne being 1275 keV and 230 e^{2}fm^4 respectively. The smaller $B(E2)$ value for ^{22}Ne leads to a significantly smaller coupling effect on the elastic scattering. In ^{17}Ne there are two low-lying resonances coupled to the $1/2^-$ ground state by $E2$ transitions, the 1.288 MeV $3/2^-$ and the 1.764 MeV

Table 1
Best-fit optical model potential parameters for 136 MeV ^{17}Ne + ^{208}Pb and 131 MeV ^{20}Ne + ^{208}Pb. The imaginary parts contain both volume and derivative Woods-Saxon terms (the notation follows Ref. [57]). Both potentials also include a fixed volume Woods-Saxon imaginary term with parameters: $W = 10.0$ MeV, $r_W = 1.0$ fm and $a_W = 0.3$ fm. The Coulomb potential radius parameter was $r_C = 1.30$ fm in both cases and $R_x = r_x \times (A_p^{1/3} + A_t^{1/3})$.

Projectile	V (MeV)	r_0 (fm)	a_0 (fm)	W (MeV)	r_W (fm)	a_W (fm)	W_D (MeV)	r_D (fm)	a_D (fm)
^{17}Ne	63.53	1.300	0.309	0.627	1.300	1.790	11.82	1.344	0.438
^{20}Ne	58.76	1.231	0.579	0.345	1.302	2.705	22.56	1.267	0.433

$5/2^-$. Two separate experimental determinations of the relevant $B(E2)$ values are available in the literature: $B(E2; 1/2^- \rightarrow 3/2^-) = 95^{+26}_{-36}$ e^{2}fm^4 and $B(E2; 1/2^- \rightarrow 5/2^-) = 179 \pm 26$ e^{2}fm^4 [53] or $B(E2; 1/2^- \rightarrow 5/2^-) = 90 \pm 18$ e^{2}fm^4 [12]. In order to make a direct comparison with ^{20}Ne and ^{22}Ne the difference in spin factors for ^{17}Ne must be taken into consideration; if this is done the equivalent $B(E2)$s for ^{17}Ne are a factor of two smaller than the actual non-spin-zero values, suggesting only a modest coupling effect compared to the stable Ne isotopes.

We thus find that while there are superficial strong resemblances between the ^{17}Ne + ^{208}Pb elastic scattering and that for other similar systems, interpreting them in terms of characteristic nuclear structure properties is not straightforward. We therefore now proceed to a theoretical analysis, beginning with optical model fits.

4. Optical model analysis

Since the 131 MeV ^{20}Ne + ^{208}Pb elastic scattering data of Gross et al. [49] most resemble the present ^{17}Ne data and many other important parameters of the two systems are similar: Coulomb barrier height, projectile charge, r.m.s. radius, incident energy, etc., we perform parallel optical model fits to both data sets. Comparison of the resulting potentials will provide some indication as to which aspect of the structure of ^{17}Ne is most important in determining the character of its elastic scattering. All calculations were performed with the code FRESCO [54].

The fits employ standard Woods-Saxon potential forms, volume for the real parts and volume plus derivative for the imaginary. This combination is essential in order to obtain the best possible fit to the ^{17}Ne data without producing unphysical cross sections in the angular range where there are no data. The resulting volume imaginary term is shallow but of long range, a characteristic it shares with semi-classical polarisation potentials for Coulomb excitation, see e.g. Refs. [55,56].

The optical model fits are shown together with the data in Fig. 3; the description is good in both cases, the χ^2/N values being 0.46 and 1.24 for ^{17}Ne and ^{20}Ne respectively. The corresponding parameter values are given in Table 1. Equivalent fits are of course possible with alternative parameter sets, but we have confirmed that the differences between the ^{17}Ne and ^{20}Ne optical potentials are robust and physically meaningful. The total reaction cross sections are 1800 mb and 1817 mb for ^{17}Ne + ^{208}Pb and ^{20}Ne + ^{208}Pb respectively, essentially identical.

In Fig. 4 the best-fit optical model potentials as a function of radius for the two systems are compared. The real part is much weaker for ^{17}Ne whereas the imaginary part is slightly stronger in the region of the strong absorption radius, approximately 13 fm for these systems. This is suggestive of a significant contribution from breakup for ^{17}Ne that is not present for ^{20}Ne, the differences between the optical model potentials being consistent with the properties of the dynamical polarisation potential generated by breakup. On the other hand, the semi-classical dynamical polarisation potential for quadrupole Coulomb excitation is essentially purely imaginary and proportional to the $B(E2)$; a comparison of the imaginary parts of the optical potentials therefore suggests that Coulomb excitation of the two low-lying $E2$ resonances in ^{17}Ne is not a major contributor.

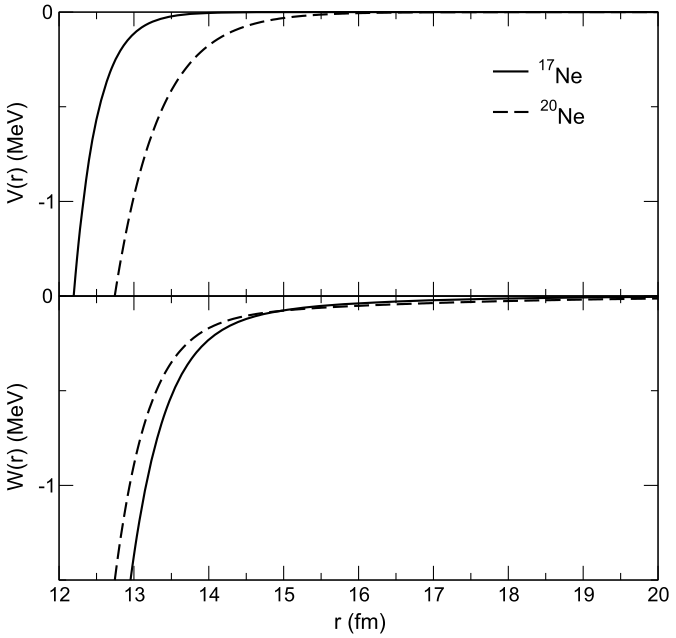

Fig. 4. Best-fit optical model potentials as a function of radius for 136 MeV ^{17}Ne + ^{208}Pb (solid curves) and 131 MeV ^{20}Ne + ^{208}Pb (dashed curves).

The optical model analysis thus points to a less important influence on the elastic scattering of ^{17}Ne of $E2$ Coulomb coupling to the low-lying $3/2^-$ and $5/2^-$ resonances than is the case for the similar $0^+_1 \rightarrow 2^+_1$ coupling in ^{20}Ne. In the next section we further investigate this by explicit coupled channels (CC) calculations.

5. Coupled channels analysis

We fit the ^{17}Ne + ^{208}Pb and ^{20}Ne + ^{208}Pb elastic scattering data with CC calculations including quadrupole couplings to the $3/2^-_1$ and $5/2^-_1$ resonances of ^{17}Ne and the bound 2^+_1 level of ^{20}Ne using the standard CC formalism [51,52]. The two ^{17}Ne resonances are thus treated as if they were bound. This should be a reasonable approximation since both levels are very narrow. In addition, the $3/2^-_1$ level can only decay by either simultaneous $2p$ emission or the emission of a γ ray; only the γ decay has been observed [53]. No evidence for simultaneous emission of 2 protons from the $5/2^-_1$ resonance has been found, only sequential decay via the ground state of ^{16}F [53].

For ^{17}Ne we use the $B(E2; 1/2^-_1 \rightarrow 5/2^-_1)$ of Marganiec et al. [12] and assume that the $3/2^-_1$ level forms part of a rotational band together with the $5/2^-_1$ and the ground state. The nuclear deformation length δ_2 was extracted from the $B(E2)$ assuming the collective model using the measured charge radius of ^{17}Ne [58]. For ^{20}Ne, the $B(E2; 0^+_1 \rightarrow 2^+_1)$ is taken from the compilation of Raman et al. [59] and δ_2 obtained by fitting the inelastic scattering data of Gross et al. [49]. Reorientation couplings are included as appropriate with strengths obtained assuming the collective rotational model. Optical potentials employ standard Woods-Saxon forms and were adjusted to give the best fit to the elastic scattering data when the inelastic couplings are included.

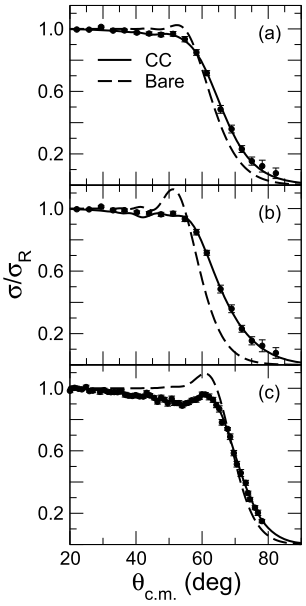

Fig. 5. (a) 136 MeV ^{17}Ne + ^{208}Pb elastic scattering compared to a CC calculation using the $B(E2)$ values of Marganiec et al. [12]. (b) 136 MeV ^{17}Ne + ^{208}Pb angular distribution compared to a CC calculation using the $B(E2)$ values of Chromik et al. [53]. (c) 131 MeV ^{20}Ne + ^{208}Pb [49] elastic scattering compared to a CC calculation using the $B(E2)$ value of Raman et al. [59]. Solid curves denote the CC fits described in the text while dashed curves denote the respective bare, no-coupling results.

The resulting fits are compared with the data in Fig. 5 (a) and (c). The solid curves denote the CC fits and the dashed curves show the effect of switching off all couplings. The difference between the solid and dashed curves thus provides a qualitative indication of the coupling effect. The fits are again good, with χ^2/N values of 1.21 and 0.66 for ^{17}Ne and ^{20}Ne respectively. The corresponding reaction cross sections are 1903 mb and 1968 mb, with total inelastic scattering cross sections of 350 mb and 627 mb. Thus, the $E2$ coupling to low-lying levels accounts for $\sim 18\%$ and $\sim 32\%$ of the reaction cross section for ^{17}Ne and ^{20}Ne respectively.

It is immediately apparent that the coupling effect is significantly smaller for ^{17}Ne. Indeed, a comparison of the solid and dashed curves for ^{20}Ne suggests that the $0^+_1 \rightarrow 2^+_1$ coupling accounts for the bulk of the coupling influence on the elastic scattering, whereas for ^{17}Ne it is clear that the quadrupole coupling to the two resonances only accounts for a relatively modest fraction since the bare, no-coupling angular distribution does not show the usual pronounced Coulomb rainbow peak, unlike the ^{20}Ne case. The CC calculations therefore seem to confirm the indications of the optical model fits: in contrast to ^{20}Ne the $E2$ Coulomb coupling to low-lying levels is not responsible for a significant part of the observed suppression of the Coulomb rainbow peak in the ^{17}Ne + ^{208}Pb elastic scattering. However, since the $B(E2; 1/2^-_1 \rightarrow 5/2^-_1)$ of Marganiec et al. [12] is about a factor of two smaller than that of Chromik et al. [53] it is necessary to check whether this conclusion depends significantly on which value is chosen. To this end a similar CC fit was performed using the Chromik et al. $B(E2)$s and the results are shown in Fig. 5 (b). We now see a substantial coupling effect, similar to that found for the $0^+_1 \rightarrow 2^+_1$ coupling in ^{20}Ne. The importance of the effect will also depend on the value of δ_2 which is not well determined for ^{17}Ne since there are no "inelastic scattering" data available with which to fix it. A test CC fit to the data using the Chromik et al. [53] $B(E2)$s but with a δ_2 80% of the "collective model" value found that while the coupling effect is slightly reduced, it is still comparable with that for ^{20}Ne.

The question of which of the $B(E2)$ values available in the literature is most accurate is thus of vital importance in determining whether the $E2$ coupling plays a significant rôle in the ^{17}Ne + ^{208}Pb elastic scattering. The measured inclusive ^{15}O production angular distribution may give some indication since it provides an upper limit on the possible cross section for excitation of the two $E2$ resonances. In fact, since the 1.288 MeV $3/2^-$ resonance has only been observed to decay by γ emission, only excitation of the 1.764 MeV $5/2^-$ is relevant to this comparison. The CC calculations produce ^{17}Ne* angular distributions in the centre of mass frame, whereas the data are for the (inclusive) ^{15}O angular distribution in the laboratory frame. The CC angular distributions were therefore transformed into the equivalent laboratory frame ^{15}O angular distributions by means of a Monte Carlo simulation of the sequential proton decay of the ^{17}Ne 1.764 MeV $5/2^-$ resonance via the (unbound) 0^- ground state of ^{16}F. The results are compared with the inclusive ^{15}O angular distribution in Fig. 6.

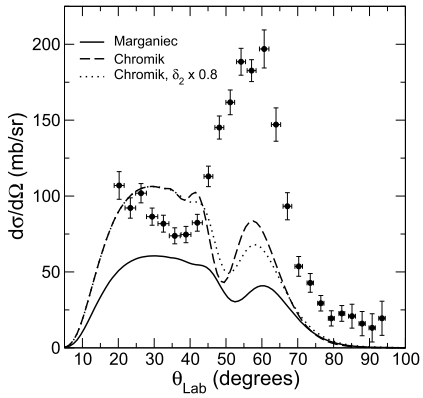

Fig. 6. Results of CC calculations of excitation of the ^{17}Ne 1.764 MeV $5/2^-$ resonance compared to the measured inclusive ^{15}O angular distribution (filled circles). The CC results were suitably transformed to the equivalent laboratory frame ^{15}O angular distribution via a Monte Carlo simulation. The solid curve denotes the result of a calculation using the $B(E2; 1/2^-_1 \rightarrow 5/2^-_1)$ of Marganiec et al. [12], the dashed curve a calculation using that of Chromik et al. [53] and the dotted curve a calculation with the Chromik et al. $B(E2; 1/2^-_1 \rightarrow 5/2^-_1)$ but a δ_2 80% of the "collective" value, see text.

Fig. 6 provides additional support for the conclusion that the $E2$ coupling to the two low-lying resonances in ^{17}Ne does not have a substantial influence on the elastic scattering, since the CC cross section for excitation of the 1.764 MeV $5/2^-$ resonance calculated using the $B(E2)$ of Chromik et al. [53] significantly over predicts the measured inclusive ^{15}O cross section at $\theta_{\rm lab} = 25^\circ$ – 40°. A definitive conclusion concerning the importance of the quadrupole coupling to these two low-lying resonances in ^{17}Ne will nevertheless require a further determination of the relevant $B(E2)$ values and/or a measurement of the inelastic scattering to the 1.288 MeV $3/2^-$ level (recall that proton decay of this level appears inhibited so that it should be possible to measure an inelastic scattering angular distribution in a conventional experiment).

6. Summary and conclusions

Angular distributions for the elastic scattering and inclusive ^{15}O production cross sections of the drip-line nucleus ^{17}Ne from a ^{208}Pb target were measured for the first time at the GANIL SPIRAL1 facility. The experiment was performed using the GLORIA detector array, providing high-resolution data over the range $\theta_{\rm lab} = 20^\circ$ to 95°. A near-barrier incident energy (136 MeV) and heavy target were specifically chosen to maximise possible coupling effects due to the Borromean nature and potential two-proton halo of the weakly-bound ^{17}Ne.

The elastic scattering data exhibit the suppression of the Coulomb rainbow peak characteristic of the influence of strong couplings. This is the first time that such an effect has been unambiguously seen for a proton halo projectile, the available data

for ^{8}B being inconclusive in this respect. Superficial similarities between the ^{17}Ne data and those for near-barrier ^{6}He and ^{20}Ne elastic scattering from ^{208}Pb suggest that $E1$ coupling to the low-lying continuum and/or $E2$ excitation of low-lying quadrupole resonances in ^{17}Ne could be responsible, but interpreting these in terms of specific nuclear structure properties is not straightforward.

A parallel optical model analysis of the 136 MeV ^{17}Ne + ^{208}Pb and 131 MeV ^{20}Ne + ^{208}Pb [49] elastic scattering data described well both angular distributions with standard Woods-Saxon potential forms. The real part consisted of a volume term and the imaginary part a surface derivative term plus a shallow, long-range volume term for both systems. The long-range volume imaginary terms have similar characteristics to semi-classical polarisation potentials simulating the effect of Coulomb excitation [55,56]. Detailed comparison of the best-fit potentials, particularly the real parts and the long-range imaginary terms, suggests that quadrupole coupling to the 1.288 MeV $3/2^-$ and 1.764 MeV $5/2^-$ resonances does not play the major rôle in the observed suppression of the Coulomb rainbow peak. It is also interesting to note that, despite the weakly-bound nature of ^{17}Ne, the deduced reaction cross section is similar to that obtained from the ^{20}Ne data.

A more detailed description within the CC framework supports the suggestion of the optical model analysis that the quadrupole coupling to the two resonances is not the main cause of the observed strong coupling effect on the ^{17}Ne + ^{208}Pb elastic scattering. While a CC calculation based on the larger of the available $B(E2)$ values [53] does show a similar influence of these couplings to that of the $0^+_1 \rightarrow 2^+_1$ coupling in ^{20}Ne, the corresponding angular distribution for excitation of the 1.764 MeV $5/2^-$ resonance significantly over predicts the inclusive ^{15}O angular distribution at forward angles. Since the inclusive ^{15}O cross section presents an upper limit for the $^{17}\text{Ne} \rightarrow {}^{15}\text{O} + p + p$ breakup cross section this result appears to be ruled out; a definite answer will require a firm determination of the relevant B(E2) values. A CC calculation using the $B(E2)$ of Marganiec et al. [12] is consistent with the main coupling effect being due to other sources, most probably $E1$ excitation to the low-lying continuum of ^{17}Ne, although confirmation of this will require CDCC calculations explicitly including the breakup couplings. Recall that ^{17}Ne also has a $1/2^+$ resonance at an excitation energy of 1.908 MeV, coupled to the ground state by an $E1$ transition, which may also play an important rôle.

The new data therefore provide an important addition to the available information on the scattering of halo nuclei, with the first unambiguous evidence of strong coupling effects for a proton halo nucleus. An initial analysis was presented, consisting of optical model and CC fits. Strong indications that the observed coupling effect is mainly due to excitation of the low-lying continuum rather than the two narrow $E2$ resonances of ^{17}Ne were found. Nevertheless, fully to understand the effects of the two-proton halo in the reaction dynamics of ^{17}Ne additional scattering data covering a wider range of energies and targets as well as resolution of the different $B(E2)$ values will be required in addition to extended CDCC calculations.

Declaration of competing interest

The authors declare that they have no known competing financial interests or personal relationships that could have appeared to influence the work reported in this paper.

Data availability

Data will be made available on request.

Acknowledgements

This work was supported by the European Union's Horizon 2020 research and innovation programme under grant agreement No. 654002, the Polish National Science Centre under the COPIN-INFN and LEA COPIGAL Collaborations, and the Spanish MICINN AEI grants Nos. PGC2018-095640-B-I00, FPA2015-64969-P and PID2019-104390GB-I00. J.D-O acknowledges the support of AEI/FEDER/EU Ph.D. fellowship BES2016-077059.

References

[1] P.G. Hansen, B. Johnson, Europhys. Lett. 4 (1987) 409.
[2] I. Tanihata, et al., Phys. Rev. Lett. 55 (1985) 2676; Phys. Lett. B 160 (1985) 380.
[3] D.J. Millener, J.W. Olness, E.K. Warburton, S.S. Hahna, Phys. Rev. C 28 (1983) 497.
[4] M. Fukuda, et al., Phys. Lett. B 268 (1991) 339.
[5] T. Minamisono, et al., Phys. Rev. Lett. 69 (1992) 2058.
[6] W. Schwab, et al., Z. Phys. A 350 (1995) 283.
[7] J. Kelley, et al., Phys. Rev. Lett. 77 (1996) 5020.
[8] M. Fukuda, et al., Nucl. Phys. A 656 (1999) 209.
[9] M.V. Zhukov, B.V. Danilin, D.V. Fedorov, J.M. Bang, I.J. Thompson, J.S. Vaagen, Phys. Rep. 231 (1993) 151.
[10] M.V. Zhukov, I.J. Thompson, Phys. Rev. C 52 (1995) 3505.
[11] C. Lehr, et al., Phys. Lett. B 827 (2022) 136957.
[12] J. Marganiec, et al., Phys. Lett. B 759 (2016) 200.
[13] J. Dobaczewski, H. Flocard, J. Treiner, Nucl. Phys. A 422 (1984) 103.
[14] O.R. Kakuee, et al., Nucl. Phys. A 728 (2003) 339.
[15] K. Rusek, et al., Phys. Rev. C 72 (2005) 037603.
[16] D. Escrig, et al., Nucl. Phys. A 792 (2007) 2.
[17] A.M. Sánchez-Benítez, et al., Nucl. Phys. A 803 (2008) 30.
[18] V. Parkar, et al., Acta Phys. Pol. B 42 (2011) 3.
[19] L. Acosta, et al., Phys. Rev. C 84 (2012) 044604.
[20] M. Cubero, et al., Phys. Rev. Lett. 109 (2012) 262701.
[21] J.P. Fernández-García, et al., Phys. Rev. Lett. 110 (2013) 142701.
[22] J.P. Fernández-García, et al., Phys. Rev. C 92 (2015) 044608.
[23] N. Keeley, K.W. Kemper, K. Rusek, Phys. Rev. C 88 (2013) 017602.
[24] Ł. Standyło, et al., Phys. Rev. C 87 (2013) 064603.
[25] K. Rusek, et al., Acta Phys. Pol. B 43 (2012) 233.
[26] I. Martel, et al., Phys. Rev. C 102 (2020) 034609.
[27] A. Barioni, et al., Phys. Rev. C 84 (2011) 014603.
[28] V. Morcelle, et al., Phys. Rev. C 95 (2017) 014615.
[29] E.F. Aguilera, et al., Phys. Rev. C 79 (2009) 021601(R).
[30] R. Spartá, et al., Phys. Lett. B 820 (2021) 136477.
[31] L. Yang, et al., Nat. Commun. 13 (2022) 7193.
[32] Y.Y. Yang, et al., Phys. Rev. C 87 (2013) 044613.
[33] M. Mazzocco, et al., Phys. Rev. C 100 (2019) 024602.
[34] P. Descouvemont, Phys. Rev. C 93 (2016) 034616.
[35] A. Pakou, et al., Phys. Rev. C 102 (2020) 031601.
[36] K. Wang, et al., Phys. Rev. C 103 (2021) 024606.
[37] Y. Kucuk, E. Aciksoz, Eur. Phys. J. A 52 (2016) 98.
[38] Meng Wang, W.J. Huang, F.G. Kondev, G. Audi, S. Naimi, Chin. Phys. C 45 (2021) 030003.
[39] I. Tanihata, et al., Phys. Lett. B 206 (1988) 592.
[40] A. Ozawa, et al., Phys. Lett. B 334 (18) (1994) 8.
[41] R. Kanungo, et al., Phys. Lett. B 571 (2003) 21.
[42] M.J.G. Borge, et al., Phys. Lett. B 317 (1993) 25.
[43] J. Casal, et al., Phys. Rev. C 94 (2016) 054622.
[44] Y. Kucuk, I. Boztosun, N. Keeley, Phys. Rev. C 79 (2009) 067601.
[45] J.J. Kolata, V. Guimarães, E.F. Aguilera, Eur. Phys. J. A 52 (2016) 123.
[46] G. Marquínez-Durán, Nucl. Instrum. Methods A 755 (2014) 69.
[47] N. Keeley, K.W. Kemper, K. Rusek, Eur. Phys. J. A 145 (2014).
[48] R. Kumar, A. Bonaccorso, Phys. Rev. C 84 (2011) 014613.
[49] E.E. Gross, et al., Phys. Rev. C 17 (1978) 1665.
[50] E.E. Gross, et al., Phys. Rev. C 29 (1984) 459.
[51] T. Tamura, Rev. Mod. Phys. 37 (1965) 679.
[52] G.R. Satchler, Direct Nuclear Reactions, Oxford University Press, 1983.
[53] M.J. Chromik, et al., Phys. Rev. C 66 (2002) 024313.
[54] I.J. Thompson, Comput. Phys. Rep. 7 (1988) 167.
[55] W.G. Love, T. Terasawa, G.R. Satchler, Phys. Rev. Lett. 39 (1977) 6.
[56] A. Baltz, S.K. Kauffmann, N.K. Glendenning, K. Pruess, Phys. Rev. Lett. 40 (1978) 20.
[57] C.M. Perey, F.G. Perey, At. Data Nucl. Data Tables 17 (1976) 1.
[58] W. Geithner, et al., Phys. Rev. Lett. 101 (2008) 252502.
[59] S. Raman, C.W. Nestor, P. Tikkanen, At. Data Nucl. Data Tables 78 (2001) 1.